



Eliminating Volatile-Induced Surface Porosity During Resin Transfer Molding of a Benzoxazine/Epoxy Blend

M. Anders*, J. Lo, T. Centea, and S.R. Nutt

M.C. Gill Composites Center, Viterbi School of Engineering, University of Southern California, 3651 Watt Way, VHE-708, Los Angeles, California, 90089, United States.

*Corresponding author's e-mail: anders@usc.edu

Abstract:

We studied the mechanism of volatile-induced surface porosity formation during the resin transfer molding (RTM) of aerospace composites using a blended benzoxazine/epoxy resin, and identified reduction strategies based on material and processing parameters. The influence of viscosity and pressure on resin volatilization were determined. Then, *in situ* data was collected during molding using a lab-scale RTM system for different cure cycles and catalyst concentrations. Finally, the surface quality of molded samples was evaluated. The results show that surface porosity occurs when cure shrinkage causes a sufficient decrease in cavity pressure prior to resin vitrification. The combination of thermal gradients and rapid gelation can generate large spatial variations in viscosity, rendering the coldest regions of a mold susceptible to porosity formation. However, material and cure cycle modifications can alter the resin cure kinetics, making it possible to delay the pressure drop until higher viscosities are attained to minimize porosity formation.

1. INTRODUCTION

Resin transfer molding (RTM) has been used to produce composite structures for aerospace applications since the early 1980s [1]. RTM is preferred for geometrically complex small to medium-sized parts that require low microstructural defect levels and excellent surface finish. The process



can also be largely automated to improve production rates and repeatability, allowing medium to high volume production of high performance composites [2].

Resin transfer molding typically consists of three stages. The first, preforming, consists of preparing the fiber reinforcement by cutting and stacking plies of dry fibers, pre-shaping them by heated compaction, and placing them within the mold cavity. The second step involves injecting a pre-catalyzed but uncured thermoset resin into the heated mold cavity and saturating the fibrous preform. The final stage consists of imposing a temperature and pressure cycle that cures the resin while suppressing the formation of microstructural defects.

Voids are the most common type of defect encountered in RTM parts. They are often a result of air trapped within the mold cavity during injection, which can occur in the form of dry spots from converging flow fronts [3], or incomplete preform saturation due to an imbalance between the capillary and bulk flows that occur within dual-scale woven preforms [4,5]. Resin infiltration can be optimized by adjusting the gate locations [6] and inlet pressure [4] to minimize air entrapment. For a given injection scheme, air-induced voids can be further eliminated by applying vacuum to the mold cavity prior to (and during) injection, flushing additional resin through the system to evacuate bubbles, and increasing the applied hydrostatic pressure during cure [7]. During typical RTM, the microstructure achieved at the end of the injection stage remains largely stable during subsequent cure.

However, in some cases, voids can also arise from a second source: volatiles released by the resin at elevated temperatures. The positive hydrostatic pressure used during RTM (in contrast to vacuum-only resin infusion processes) was first developed to suppress the volatilization of water during the condensation cure of phenolic resins [1,8]. The source of volatiles is not limited to byproducts of polymerization – gas release can also occur due to residual solvents, vaporized



monomers, dissolved air and moisture, degradation byproducts, or other impurities/contaminants. The detection, analysis, and control of volatile-induced porosity is particularly challenging because voids can form after injection, at any point during the cure stage.

1.1. Literature Review

Voids in thermoset matrix composites are known to be detrimental to both mechanical properties [9] and cosmetic appearance [10]. However, while multiple studies have addressed the formation of voids during resin injection, relatively few studies have been devoted to the topic of void behavior during the curing stage of RTM.

The major void modeling approaches for thermoset composites derive from studies by Kardos et al. [11] and Wood and Bader [12]. Kardos et al. [11] developed a model for void nucleation and growth in the context of autoclave processing with an epoxy resin. They considered a diffusion-based mechanism, and assumed water to be the primary diffusible species. The model described both voids that exist initially at the onset of cure (and contain dry air or an air/water mixture), and voids that nucleate spontaneously at supersaturated conditions and contain only water vapor. They predicted a strong influence of initial dissolved moisture concentration on final void size and pressure. Furthermore, they noted that void growth cannot occur if the void gas pressure exceeds the saturated vapor pressure of the volatile species dissolved in the resin, and constructed a “stability map” showing the resin pressure required to suppress void growth as function of temperature and dissolved moisture content. Wood and Bader [12] described a similar diffusion-based model for void growth in autoclaved epoxy laminates, which instead considered nitrogen as the primary diffusible species. By experimentally determining surface tension, dissolved gas concentration, and the gas diffusion coefficient, they were able to predict time-dependent changes in bubble radii. Ledru et al. [13] developed a visco-mechanical void growth model (also in the context of epoxy-matrix



composites cured by autoclave), which described a time-dependent void radius as a function of external pressure, temperature, viscosity, and surface tension, for voids containing a fixed amount of gas (i.e. omitting diffusion effects). They subsequently coupled the visco-mechanical model with a (water) diffusion-based model [14], aiming to improve upon previous diffusion-based models by accounting for viscosity and polymer crosslinking effects and by refining the predicted influence of hydrostatic pressure. They noted that, compared to diffusion-only models, visco-mechanical phenomena reduce void size. Like Kardos, they reported that initial dissolved volatile concentration and applied pressure were the most significant factors for void size, but they encountered difficulties in confirming the diffusion coefficient (which also strongly influences model predictions).

While the studies referenced in [11–14] consider autoclave processing, Lundström confirmed that, in resin transfer molding processes, hydrostatic pressure can also cause gas dissolution and can collapse voids entirely [15]. The concentration of volatile species initially present in the resin also can be reduced prior to injection by vacuum-degassing [16], but the effectiveness of this technique is limited by the resin pot life, since degassing requires low viscosity and thus must be performed at high temperatures. Various time/temperature/vacuum pressure combinations can be used to influence the amount of volatiles extracted, but excessive vacuum-degassing increases the risk of pre-curing the resin, which can shorten the pot-life and complicate resin injection.

The volumetric change of thermoset resins during cure has been associated with defect formation. Eom et al. showed that, in three-dimensionally constrained thermoset resin, internal tensile stresses can develop due to chemical cure shrinkage, leading to void formation [17]. Furthermore, they found a critical stress criterion and developed process windows, providing guidelines to prevent void formation in autoclaved glass/epoxy laminates [18]. Similarly, Wisnom et al. [19] studied the effects of thermal and chemical volumetric changes on residual stresses in



prepreg laminates, noting that it is possible for significant stresses to develop due to tool-part interactions before vitrification and even before gelation, where the resin may have a very low shear modulus but an appreciable bulk modulus. Merzlyakov et al. [20] also measured stresses in constrained thermoset resin during cure, finding that cure-induced tensile stresses were lower than expected, due to cohesive failure of the resin in the gelled (rubbery) state.

Cure shrinkage can be measured by monitoring sample thickness between parallel plates on a rheometer [21], using a pressure-volume-temperature (PVT) analyzer [22], by a gravimetric method [23], or by other methods [24]. The effects of resin volumetric changes on cavity pressure in RTM have been described by Kendall et al. [25], who noted pressure increases due to thermal expansion, as well as pressure drops attributed to cure shrinkage. Haider et al. [10] observed similar pressure drops due to cure shrinkage in automotive RTM panels, and correlated these with an increased surface roughness. Their unsaturated polyester resin exhibited much greater cure shrinkage (7-10%) than epoxies, which was successfully compensated by including a thermoplastic low profile additive (LPA). The expansion of LPA after gelation acted to reestablish positive mold pressure, resulting in high-gloss “class A” surface finishes. Boyard et al. [26] also noted increased surface roughness due to shrinkage-induced pressure drops in unsaturated polyester bulk molding compound (BMC), and used a dilatometer to develop a model for predicting cavity pressure. Recently, Landry and Hubert [27] described similar surface roughness due to shrinkage in thermoplastic short-fiber PEEK composites, developed a model to predict the pressure distribution, and correlated surface defects in colder zones with local pressure drops due to non-uniform shrinkage [28].

While the studies in the previous paragraph describe shrinkage-induced defects similar to those in our study, they differ in that none of the matrix materials exhibited significant volatility. For resins that can off-gas under deficient pressure, shrinkage-induced surface defects manifest as bubbles



instead of increased roughness. This distinctive type of defect is particularly challenging to diagnose, since it can easily be mistaken for porosity due to air (trapped during injection) unless *in situ* observations are used to identify the nature of the porosity formation. Lab-scale RTM tools have been used previously to observe in-mold volatile release, for example by Pupin et al. [29]. Their “Nano RTM” contained a glass window, allowing *in situ* observations of volatile release in a phenolic resin. The primary volatile species was water – a byproduct of the phenolic condensation reaction – which was produced in such quantities that pressure alone could not suppress void nucleation. Void-free parts were obtained by removing the water via vacuum-degassing within the mold until gelation. The volatility of our resin, in contrast, is due primarily to residual solvent, which can be forced to remain dissolved in solution using only modest pressures. However, due to resin cure shrinkage, maintaining mold cavity pressure is not always possible. The combined effects of shrinkage-induced pressure drops and high resin volatility led to the topic of this work: volatile-induced surface porosity.

In this study, we consider the RTM processing of a blended thermoset resin consisting of benzoxazine and epoxy components. This combination is being investigated (by a commercial resin supplier) for structural aerospace applications due to expected improvements in high-temperature performance. Blending benzoxazine with epoxy has been shown to increase cross-link density compared to pure benzoxazine, increasing both the T_g and toughness [30,31]. This copolymer offers a compromise, in terms of both cost and maximum service temperature, between standard aerospace epoxies and ultra-high-temperature resins such as bismaleimides (BMIs) and polyimides. However, the complex polymer chemistry results in comparatively complex in-process behavior, particularly in terms of increased volatile release during cure. If not properly controlled, this volatility can result in significant surface porosity on molded parts (shown in Figure 1), preventing the production of



laminates with high quality surface finishes. During this study, several resin formulations are used to relate changes in resin properties to in-process behavior and final part quality. These experimental variants are produced in batches in lab-scale conditions. As a result, while the formulations may not be as optimized as a commercial product, they form a representative set of model materials that make it possible to study volatile-induced porosity by demonstrating key phenomena. The study in turn enables the development of guidelines applicable to similar resin systems.

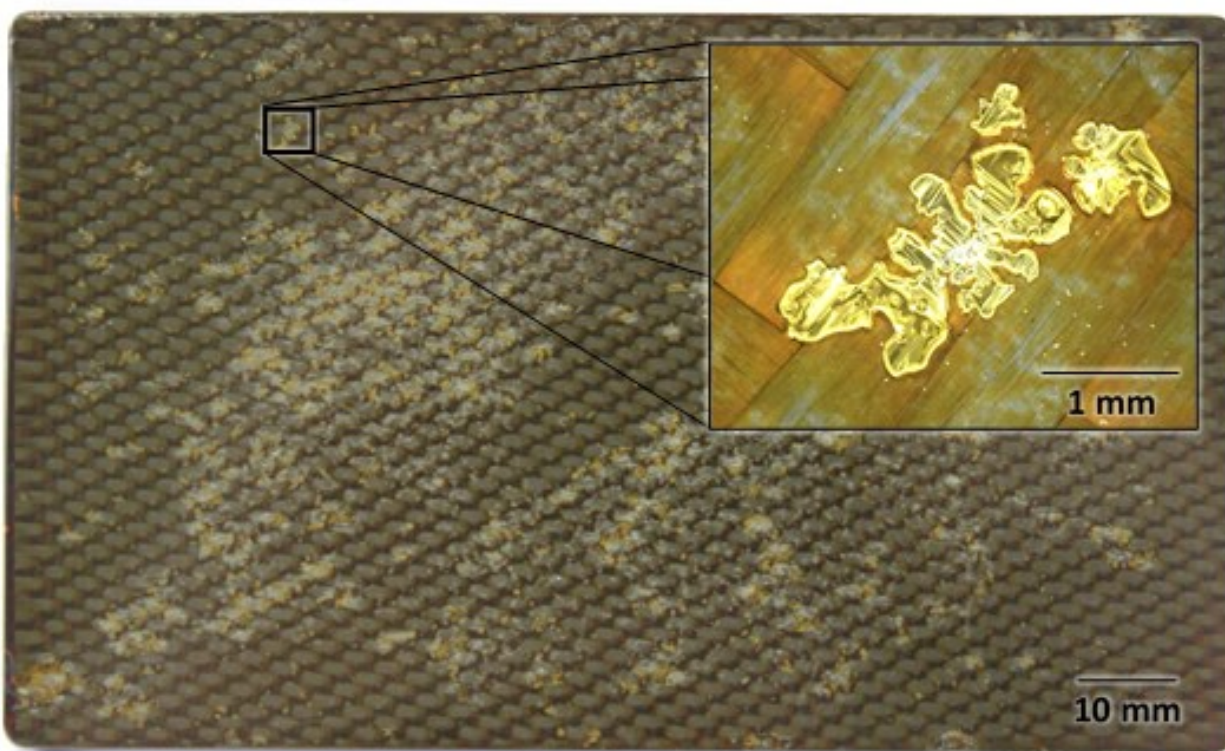


Figure 1: A laminate surface with extensive volatile-induced porosity.

This study is part of a larger ongoing research effort [32,33] that includes a companion study, which focused on several aspects of the thermochemical evolution and in-process behavior of a baseline formulation of this resin [34]. The primary volatile species was identified by Fourier transform infrared spectroscopy (FTIR) as ethyl acetate, a residual solvent used in the synthesis of the resin. While benzoxazines are traditionally known to exhibit low volatility, the experimental



formulations supplied for our work were prepared using an alternative method that avoids the need for more hazardous solvents. The drawback of this approach is that the ethyl acetate solvent cannot easily be removed prior to cure FTIR analysis of the volatiles also indicated the presence of water, but a vacuum-degassing pretreatment was shown to reduce the amount of volatilized water below the detectability limit in the FTIR signal. At higher temperatures ($>170^{\circ}\text{C}$), monomers and monomer fragments (reaction intermediates and/or degradation products) were also observed to volatilize to some extent, although the precise relative abundances of the various species were not ascertainable by FTIR. The cure shrinkage of the resin was measured by a modified pycnometry approach [33], chosen because volatile release during cure at ambient pressure precludes the use of most traditional methods. The volumetric shrinkage due to polymerization, with negligible mass loss, was shown to be about 2%.

1.2. Objective and Approach

Despite the prior studies cited above, the causes of volatile-induced surface porosity during liquid molding of such resins remain unclear, and effective strategies for avoiding defect formation must be identified. Consequently, our primary objective in this study is to clarify the connections between in-process resin behavior, temperature and pressure processing conditions, mold characteristics, cure phenomena, and surface porosity.

The porosity described herein is more complex than the more commonly studied porosity due to air and water, since there is an additional causative species: a residual solvent. The behavior differs in that the ethyl acetate is entirely soluble in the resin – in contrast to the limited solubility of air – and bubbles can very rapidly nucleate and grow, or shrink and collapse, due to changes in applied pressure. Thus, in this study, our approach consisted of experimentally investigating process phenomena, identifying a minimum “safe pressure” to prevent void nucleation and growth, and



exploring process conditions that complicate pressure control for the RTM of such materials. Based on these insights, a time-dependent void growth model can be developed. However, the required input parameters may be more difficult to determine than those for only air and water, due to the greater chemical complexity of the species causing porosity.

First, we investigated the mass stability of the resin and its relationship to viscosity by thermogravimetric analysis (TGA) and rheological dynamic analysis (RDA). Second, the in-mold behavior of the resin at various cure pressures was analyzed by fabricating neat-resin molded samples in a highly-instrumented lab-scale RTM tool, which includes a transparent tool plate to enable visual observation of the mold cavity throughout processing. Finally, the formation of surface porosity during the processing of carbon fiber-reinforced molded samples was investigated by fabricating samples within the same RTM tool.

Combining temperature, pressure, and viscosity data with direct *in situ* observation capabilities provides a powerful set of tools to understand the mechanism behind the formation of surface porosity. The results show that there exists a critical viscosity above which volatilization ceases, and a critical hydrostatic pressure above which volatile release and void formation are suppressed. If the resin pressure falls below the critical value during cure, before the viscosity attains its critical value, void growth occurs. Such a condition can occur due to the complex combined action of chemical cure shrinkage and thermal gradients, which renders the coldest surface of the part susceptible to void growth. By describing this distinctive void formation process in detail, we clarify the processing conditions that cause volatile-induced surface porosity and identify potential material and process modifications that can reduce or eliminate such defects during RTM.



2. EXPERIMENTAL METHODS

2.1. Materials

The resin selected for this study consists of benzoxazine and epoxy constituents as well as a catalyst used to accelerate the cure reaction. The resin is designed for vacuum degassing and injection at 110°C followed by cure at a nominal temperature of 185°C, though modified thermal cure cycles are possible. The nominal recommended cure pressure is 450 kPa. A free-standing post-cure for 30 minutes at 220°C is recommended to maximize mechanical properties, but is not considered in this study because the porosity formation phenomena of interest occur earlier, during in-mold processing.

Three formulations were prepared, with varying catalyst concentrations to modify the in-process behavior of the resin. The catalyst was used to accelerate the reaction, but did not affect the chemical composition of the matrix constituents. The baseline formulation contained 0.1% by weight, while the subsequent formulations contained 1% and 2% catalyst by weight, respectively. These three formulations are henceforth designated F1, F2, and F3, in order of increasing catalyst concentration. The baseline formulation, F1, was used throughout the study to identify the effects of pressure and the mechanical state of the resin on volatile release, whereas the F2 and F3 formulations were used to modify the cure kinetics during composite manufacturing tests, as outlined in Tables 1 and 2.

The fiber bed selected to mold composite samples consisted of a five-harness satin (5HS) carbon fiber fabric (Sigmatex Ltd.) with an areal weight of 364 g/m² and a 3000 fiber/tow count. The fabric included a thermoplastic binder to facilitate preforming and placement into the mold cavity.



Table 1: Thermal characterization tests.

Test set	Test type	Temperature cycles	Formulation
Linear ramps	RDA, TGA	35 - 250°C at 1, 2, 3°C/min	F1
Realistic cycles	RDA	Cycle A ^a , Cycle B ^b	F1, F2, F3
Pot life	RDA	110°C for 8 hours	F1, F2, F3

a. Cycle A = 2°C/min to 185°C, 90 min dwell

b. Cycle B = 2°C/min to 130°C, 180 min dwell, 2°C/min to 185°C, 90 min dwell

Table 2: Processing parameters for molded samples fabricated in the lab-scale RTM.

Type	Injection parameters		Cure parameters		Formulation
	Pressure (kPa)	Temperature (°C)	Pressure (kPa)	Temperature (°C)	
Neat resin	300	110	101, 160, 200, 450	170, 185, 200	F1
Composite	300	110	450	Cycle A ^a , Cycle B ^b	F1, F2, F3

a. Cycle A = 2°C/min to 185°C, 90 min dwell

b. Cycle B = 2°C/min to 130°C, 180 min dwell, 2°C/min to 185°C, 90 min dwell

2.2. Thermal Characterization

Thermogravimetric tests were performed with resin formulation F1 (using a TA Instruments Q5000IR) to determine the volatile-induced mass loss. Samples weighing 40 ± 0.5 mg were cured under atmospheric pressure, by increasing the temperature from 35°C to 250°C at rates of 1, 2, and 3°C/minute.

The resin viscosity was measured with a rheometer (TA Instruments AR2000ex), with disposable aluminum parallel-plate fixtures and an environmental test chamber (furnace) accessory. All tests were performed in oscillatory mode at 5 Hz and with a 500µm gap. The test procedure was designed to capture the material behavior before and after gelation by measuring the absolute magnitude of the complex viscosity, which is dominated by viscous behavior (i.e. the loss modulus G'') pre-gelation and becomes dominated by elastic behavior (i.e. the storage modulus G') as the resin approaches the later stages of cure. Prior to gelation, 1% strain was chosen as the controlled variable. To remain within the torque limit of the instrument upon resin gelation, a cross-over



condition corresponding to a viscosity greater than 1000 Pa·s was set, at which point the program control mode switched to torque-control at 500 μ Nm.

Rheological dynamic analysis (RDA) tests were performed in three sets, as summarized in Table 1. The first set of RDA tests consisted of linear temperature ramps with formulation F1 identical to those carried out by TGA. A second set of tests consisted of cure cycles designed to approximate the measured molding conditions described below. Finally, the viscosity of each formulation was measured for 8 hour isothermal holds at the manufacturer's recommended injection temperature of 110°C to compare the expected pot life. The pot life of the F1 formulation was >8 hours at the injection temperature, while the pot lives of F2 and F3 were ~5 and 4 hours, respectively.

2.3. Molding

2.3.1. Lab-Scale RTM System

The lab-scale RTM tool built for this study is shown in Figure 2. The main body of the mold was an anodized aluminum block containing inlet and outlet ports with “line injection” grooves used to generate a one-dimensional flow front. A “picture frame” plate with a rectangular cavity was placed against the main body to define the thickness (3.2 mm) and in-plane dimensions (76 × 127 mm) of the part. The second tool face was a 20 mm thick tempered glass plate, rated for pressures up to 1200 kPa. This glass plate formed a rigid window that allowed direct *in situ* observation of in-mold phenomena, including air evacuation and preform saturation during injection, and the time and location of any subsequent void formation.

The temperature control system of the RTM tool consisted of a K-type thermocouple (OMEGA Engineering Inc.), a PID controller (Watlow EZ-ZONE® model PM6R1CA), and two 300 W heating rods embedded through the length of the main tool body. A pressure transducer (GP:50 NY Ltd., model 131) was mounted at the center of the aluminum tool face. Temperature and pressure data



were recorded with a cRIO-9076 data acquisition system (running LabView 2012, National Instruments). Additional ports were included in the main tool body to allow for alternative thermocouple placement and the addition of other transducers (such as dielectric cure monitoring sensors). However, such sensors were not used in this study. Visual data through the window was recorded during both injection and cure. At the macro-scale, a DSLR camera (Canon EOS Rebel T1i) and the intervalometer feature of Magic Lantern (v2.3), a third-party open source software add-on, were used to capture full-field views of the molded part. At the micro-scale, a low-magnification portable USB microscope (Dino-Lite model AD4113T) was used to obtain high-resolution images.

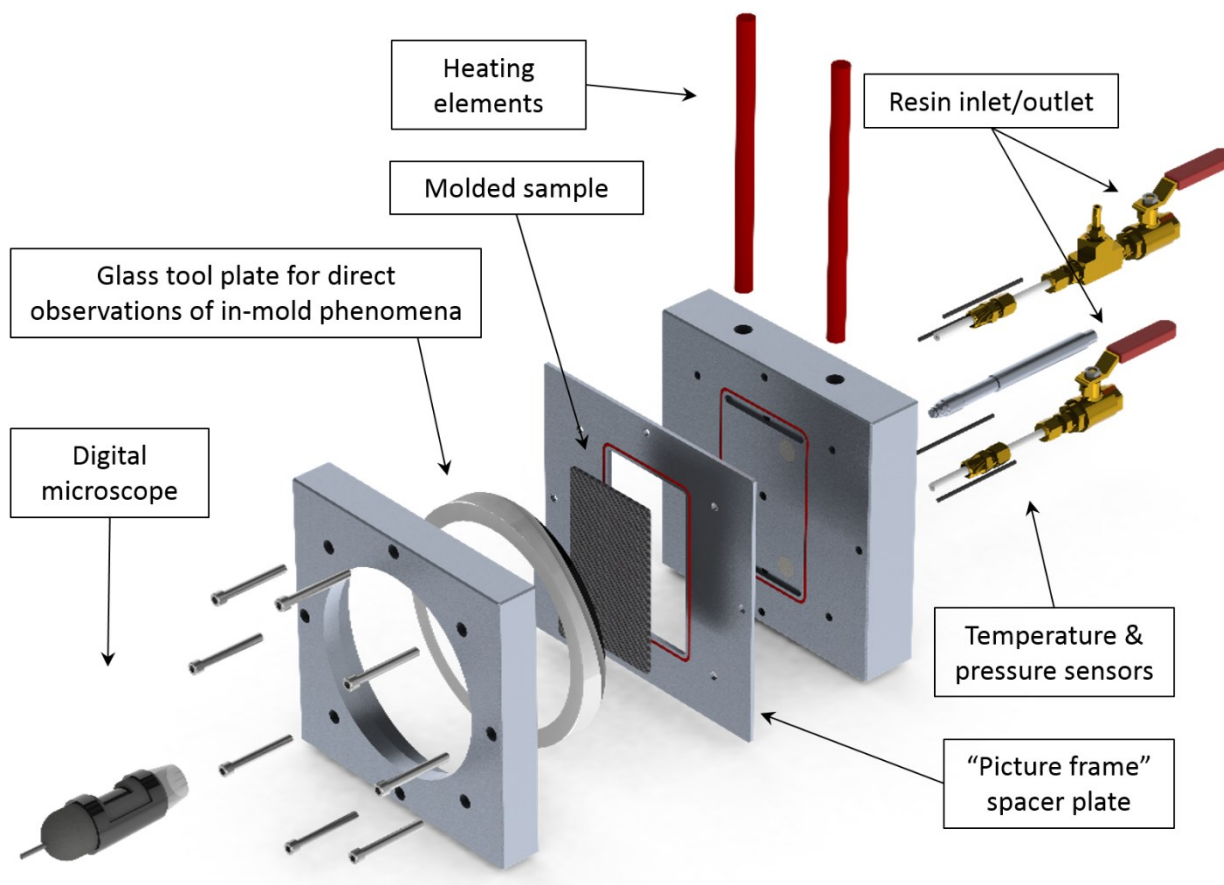


Figure 2: Exploded view of lab-scale RTM tool.



The placement of the heating rods was designed to minimize in-plane temperature gradients, but the nature of the overall geometry – with a glass tool-plate on one side – creates an inevitable through-thickness temperature gradient. During the molding of composite samples, the temperature histories were measured directly at both the hot and cold sides of the tool, for at least one sample with each cure cycle, by placing additional thermocouples into each side of the mold cavity between the preform and the mold walls.

2.3.2. *Neat Resin Samples*

Molded neat-resin samples were fabricated using the F1 formulation under various temperature and pressure conditions to analyze the pressure dependence of volatile release and void formation. No reinforcing preform was used in these tests to allow observation of bubble growth through the entire sample thickness.

The tool surfaces were coated with a liquid mold release agent (Frekote 770-NC, Henkel Inc.) prior to sealing the mold. To minimize spatial temperature gradients, two layers of fiberglass insulating fabric were wrapped around the RTM. A hole was cut in the insulation in front of the window, and a second glass plate was clamped over it to act as a heat shield while preserving transparency into the mold cavity.

Prior to injection, the resin was vacuum-degassed for 45 minutes at a reduced pressure of 6 kPa and at the nominal injection temperature of 110°C. While this procedure removed entrapped bubbles and some of the dissolved volatiles from the resin, it was not possible to remove the residual solvent entirely. Increased degassing times and temperatures were found to provide diminishing returns and to increase the risk of pre-curing the resin.

Injections were performed at 300 kPa and 110°C with a pneumatic injector (Radius 2100cc). Vacuum was applied to the cavity both before and during injection using an external vacuum pump.



Excess resin was flushed through the outlet port until no bubbles remained in the outlet tubing or in the cavity, as observed through the window.

After injection, a constant hydrostatic pressure was applied to the system by closing the outlet valve, leaving the inlet valve open, and setting the pressure to a desired level on the injector. Pressures of 101 (ambient), 160, 200, and 450 kPa were applied. The cure temperature cycles consisted of 2°C/minute ramps to isothermal holds at 170, 185, or 200°C for 120 minutes. All molding tests are summarized in Table 2.

2.3.3. *Composite Samples*

Composite panels were manufactured with all three formulations using 8 layers of carbon fabric set in a quasi-isotropic layup. Injection procedures were identical to those of the neat resin samples, and the post-fill packing pressure was set to 450 kPa for all tests. Two cure temperature cycles were used. The baseline, Cycle A, consisted of a 2°C/min ramp to 185°C followed by a 90 min dwell. A modified cure cycle, Cycle B, included an intermediate 180 min hold at 130°C before the high-temperature dwell. The measured temperature profiles during these tests were accurately replicated using combinations of ramps and holds within the rheometer to determine the evolution of the resin viscosity.

2.3.4. *Porosity Assessments*

The time of porosity formation was determined through time-lapse videos recorded at 30 s intervals, at the macro-scale by DSLR camera and at the micro-scale by USB microscope. Micro-scale visual data allowed precise timing to be determined for the formation of voids that were too small to be observed otherwise, while macro-scale data was used to confirm that the microscope observations were representative of the entire sample.



After de-molding, high-resolution photographs of the surfaces of each sample were used to quantify surface porosity. An open-source image processing software (ImageJ v1.48) was used to create binary maps of high and low porosity zones for quantifying the percent defective area on the surface of each sample. Due to the variations in appearance of surface voids (which can manifest as pits on the surface or as subsurface bubbles) and the high reflectivity of subsurface carbon fibers, a semi-automated method was used, which combined automatic selection and manual confirmation of defects.

3. RESULTS AND DISCUSSION

3.1. TGA and RDA Data

In Figure 3, we compare the TGA and RDA data for linear temperature ramps with resin formulation F1. The temperature range is truncated to the region of interest for clarity. The TGA data is expressed as a unit-less ratio of the instantaneous sample mass to the initial mass. The RDA data shows the absolute magnitude of the complex viscosity.

The rate of mass loss due to volatilization increased with temperature, until it abruptly halted due to resin solidification. The faster temperature ramps exhibited lower total mass loss, because there was less time for volatiles to evolve. However, all samples exhibited between 11% and 13% mass loss, a large amount compared to traditional RTM resins [2]. Note that as these tests were performed at ambient pressure, they represent a “worst case scenario” for RTM processing in which the mold is not pressurized. Furthermore, the TGA tests differ from in-mold processing conditions in that the samples have a free surface (and a large surface area to volume ratio) exposed to a purge gas over which evaporation could occur, whereas within an RTM, volatile voids must first nucleate and are thus also influenced by constraining fibers, surface tension, and other factors. It is therefore



not the total amount of weight loss by TGA that is comparable to RTM processing (and relevant for our purposes), but rather the state of cure at which volatile release can no longer occur. The volatilization behavior of the baseline formulation was studied and is described in greater detail in a companion paper [34].

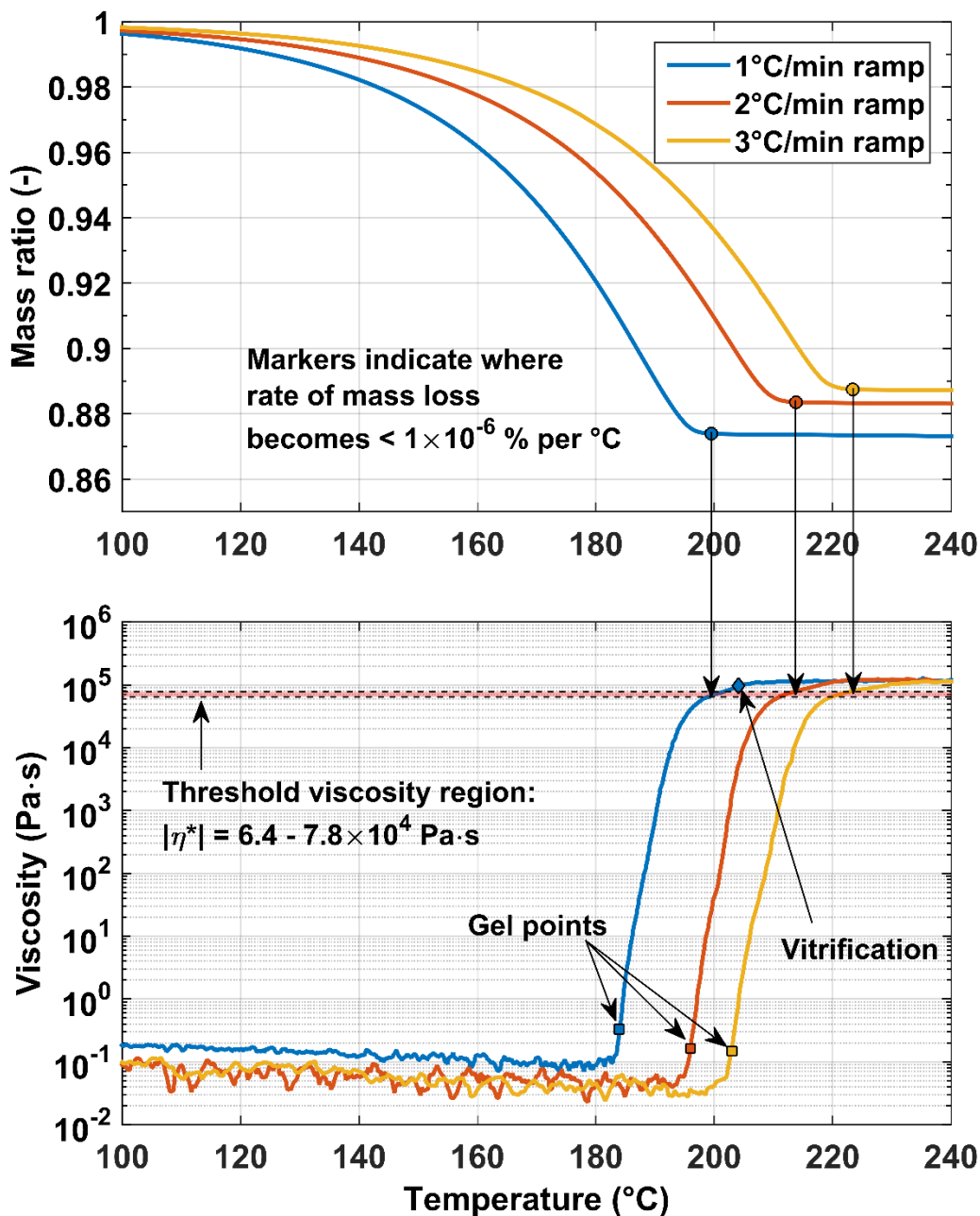


Figure 3: Mass ratio and viscosity for linear temperature ramps.



The resin viscosity remained low ($<0.2 \text{ Pa}\cdot\text{s}$, the lower detectability limit using this geometry and set of test parameters) up to temperatures of $185 - 205^\circ\text{C}$ (depending on ramp rate). In that range, the viscosity exhibited a rapid six order-of-magnitude increase, until finally stabilizing at $\sim 1.2 \times 10^5 \text{ Pa}\cdot\text{s}$. The approximate gel points, estimated using the common $G'-G''$ crossover condition, are indicated by square markers. A full frequency-sweep analysis was not performed to determine the “critical gel” time at which $\tan \delta = G''/G'$ becomes frequency independent [35]. However, additional tests at 1 Hz and 30 Hz showed similar behavior and resulted in gel times that varied by no more than 3 minutes. A rapidly increasing storage modulus (compared to the more slowly increasing loss modulus) caused the crossover to occur at relatively low absolute values of complex viscosity. Note that, after gelation, since the resin is no longer a liquid, the complex viscosity values are primarily a measure of the increasing elastic (storage) modulus of the resin. The evolution of this curve provides a convenient method for estimating the effect of cure on the mechanical state of the resin. The $1^\circ\text{C}/\text{minute}$ test exhibited a peak in $\tan \delta$ centered at 204°C (indicated by the diamond marker), which can be used to estimate the time of vitrification, as described by Bilyeu et al. [36]. No such peak was observed at higher ramp rates, likely because the temperature was increased too quickly for the glass transition temperature T_g to ever exceed the imposed temperature. For the RDA tests corresponding to molded samples (section 3.3), vitrification occurred at or near isothermal conditions, and was clearly detectable by a peak in $\tan \delta$.

The combined TGA and RDA datasets can be used to identify the resin state at which mass loss ceases. In Figure 3, the cessation of mass loss is related to a corresponding viscosity. Interestingly, these “critical viscosities” reside within a narrow band, irrespective of ramp rate, suggesting that there exists a threshold mechanical state above which volatilization can no longer occur. This state is reached just before vitrification (certainly no later, since the mobility of potentially volatile



molecules becomes greatly reduced when the polymer network transitions to a glassy phase). Note, however, that mass loss can continue past the gel point, well into the rubbery phase. A value of 7×10^4 Pa·s is used in section 3.3 as a conservative estimate for the critical viscosity, corresponding to the 2°C/min ramp rate used in the temperature cycles for all molded samples.

3.2. Neat Resin Sample Data

The neat resin panels were manufactured without entrapping air during injection. The test results are summarized in Figure 4 as a process map relating cure temperature, imposed mold pressure, and defect growth [11]. Each point represents one sample. Temperature and pressure combinations that resulted in the generation of voids are shown in red, while samples that did not grow voids are shown in blue. In cases when voids did develop, they nucleated on the hottest side of the mold cavity (the tool side that contains the heating elements), grew rapidly, sometimes detached and floated upwards, and eventually were fixed in place when the resin gelled. Figure 5 shows an example of void growth as observed *in situ* for a sample cured at ambient pressure (the circular object visible in the background is a plug in the tool plate, which provides the option to install additional sensors).

All samples cured at ambient pressure exhibited significant void growth and averaged ~10% bulk porosity by weight (compared to a void-free reference sample). Implying, not that 10% of the resin in the cavity vaporized, but rather that enough gas was released to occupy 10% of the cavity volume. The small sample cavity and lack of constraining fiber preform allowed bubbles to grow by displacing still-liquid resin (which was pushed out of the open vent). However, with a closed vent and cavity pressure provided through the inlet, pressures above approximately 200 kPa effectively suppressed void nucleation. The exact critical pressure for void suppression exhibited a mild temperature dependence, since tests at 160 kPa developed bubbles at 200°C but not 170°C. Overall, the threshold pressures required for the temperature range of interest were well within the limits of



almost all standard RTM systems. A conservative value of 200 kPa was chosen as a “critical pressure” criterion, below which void nucleation and growth can be expected during cure. Furthermore, these results were used as guidelines for the processing of the carbon fiber reinforced samples described in the following section. Specifically, an imposed pressure of 450 kPa, which is more than twice that required to suppress volatilization, was chosen to ensure that no bulk voids formed during cure. Although not described here in detail, fiber-reinforced samples cured at ambient pressure did exhibit void growth similar to neat-resin samples, with significant porosity appearing primarily in the resin-rich zones between fiber tows. However, elevated pressure was equally effective in preventing volatilization through the bulk of reinforced samples as in neat resin samples.

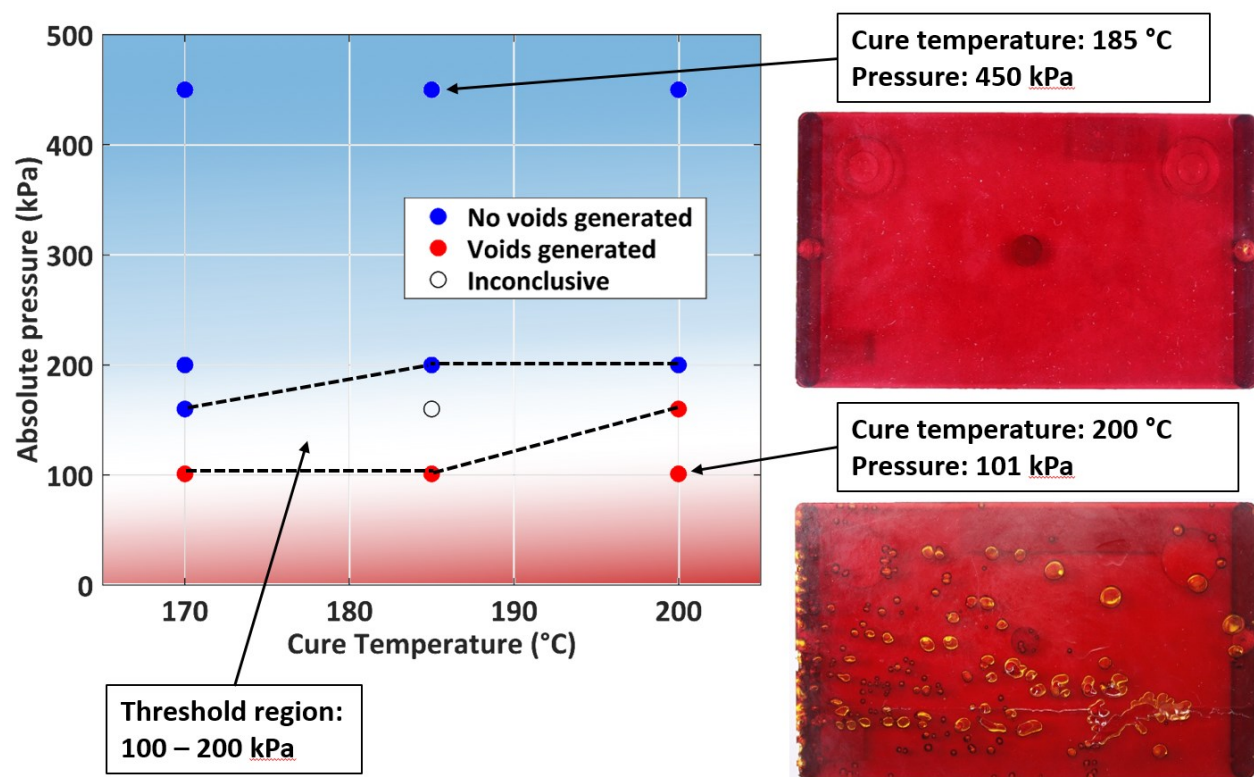


Figure 4: Temperature/pressure map of neat-resin tests. Red indicates conditions that lead to void growth, while blue corresponds to conditions that suppress void growth. Points correspond to individual tests and background shading is used to highlight the general trend.

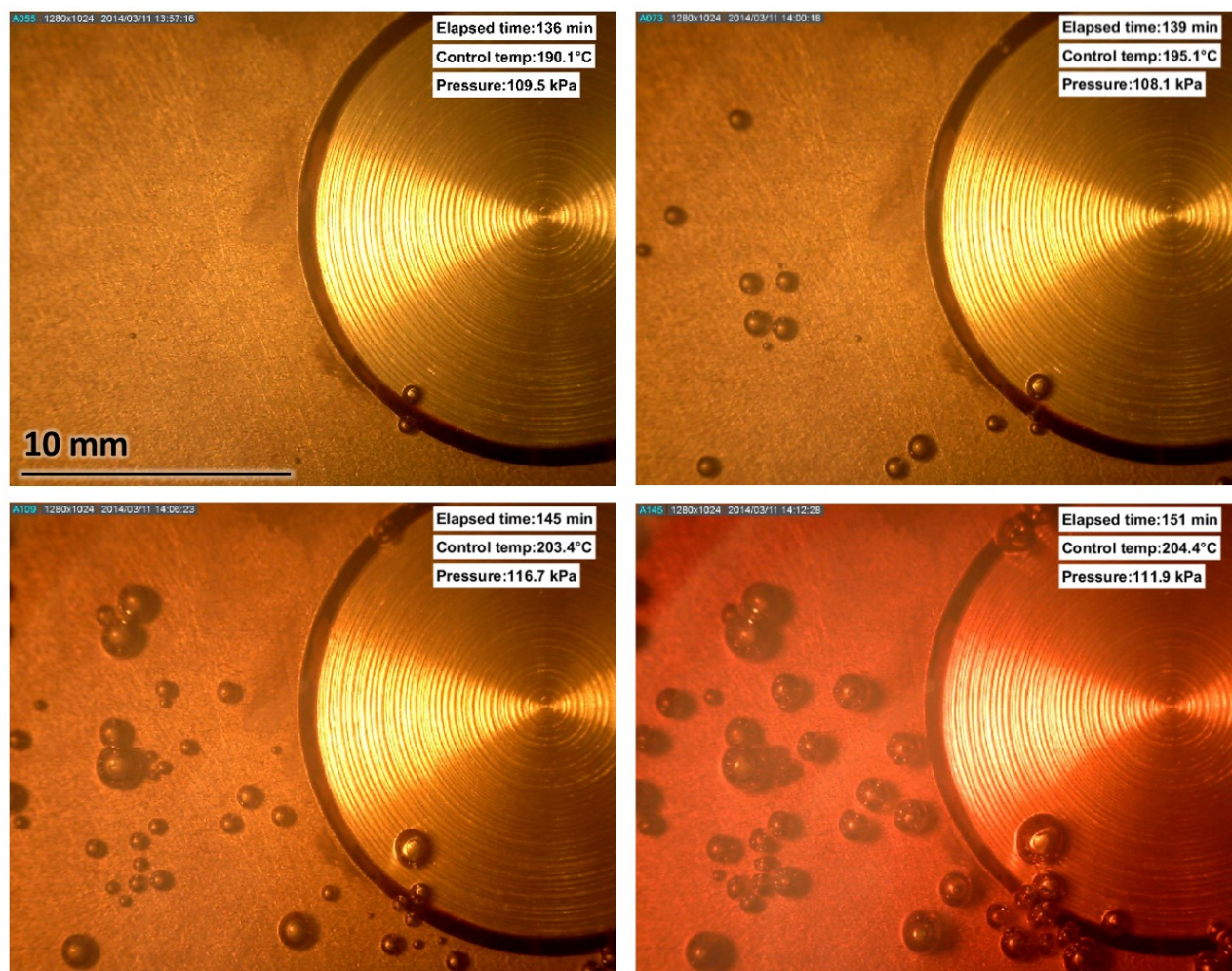


Figure 5: In-situ observations of bubble nucleation and growth in resin cured at ambient pressure.

3.3. Surface Porosity

Despite sufficient applied pressure, surface porosity developed exclusively on the colder side of all manufactured samples. The window in the mold afforded visual confirmation that, initially after injection, the surfaces of all samples were bubble-free. However, porosity developed on the window side during high-temperature dwells late in the cure cycle. The aluminum tool-side (which was slightly hotter, since it contained the heating elements) had effectively no defects for all samples, and micrographs of polished cross-sections confirmed that internal porosity was also negligibly low. For this reason, only the quality of the cold sides is considered in the subsequent description.

Please cite this article as: M. Anders, J. Lo, T. Centea, and S.R. Nutt, “Eliminating Volatile-Induced Surface Porosity During Resin Transfer Molding of a Benzoxazine/Epoxy Blend”, *Composites: Part A* 84 (2016) 442-454. DOI: <http://dx.doi.org/10.1016/j.compositesa.2016.02.024>



Table 3 summarizes the percent defective area of the cold side of each sample. Increased catalyst concentrations resulted in reduced surface porosity, and cure cycle B (which included an intermediate 3-hour dwell at 130°C) produced superior surface quality compared to the baseline, Cycle A. Figure 6 consists of representative images of cold-side laminate surfaces, in both full color and binarized forms. The thermocouple used to directly measure the window-side temperature history is visible in the first image.

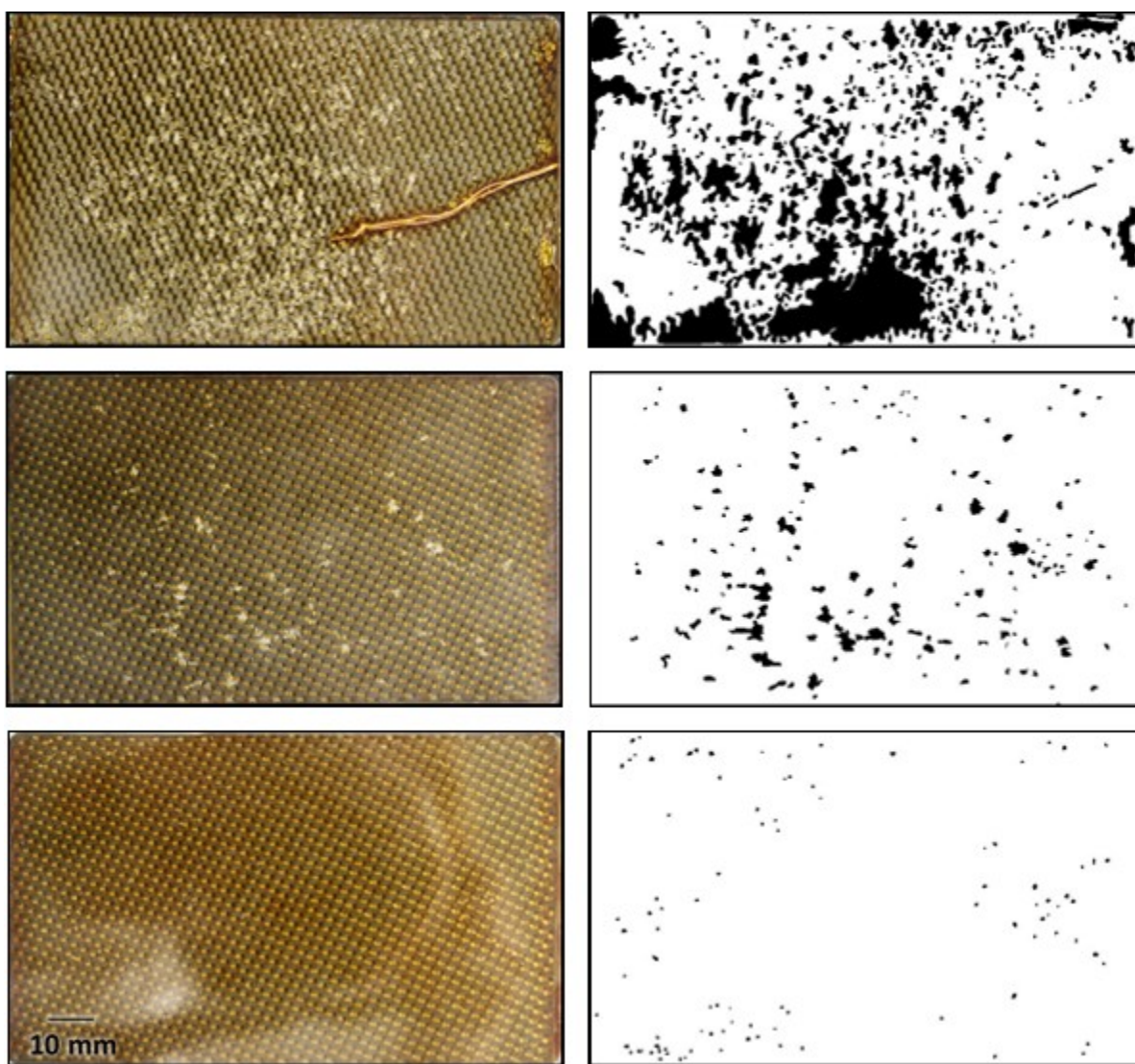


Figure 6: Some examples of surface porosity quantification by image binarization and measurement of the percent defective area. The top row is formulation F1, cycle A, the middle row is F2, cycle A, and the bottom row is F2, cycle B. The thermocouple used to measure the window-side temperature history is visible in the first image.



Table 3: Percent defective surface area for the cold sides of molded laminates.

	Formulation		
	F1	F2	F3
Cycle A	26.0%	3.32%	3.48%
Cycle B	36.8%	0.44%	0.17%

3.3.1. In Situ Data and Porosity Formation Mechanism

Figure 7 shows the measured sensor data for a composite sample with significant porosity (formulation F1 cured under Cycle A, 26% defective area). The temperature graph consists of the controller temperature (black) and the temperatures of the hot and cold sides of the mold cavity (in red and blue, respectively). The hot side, being closest to the heating elements, followed the control temperature to within 1°C, while the cold side lagged by roughly 4 minutes (or, equivalently, 8°C) during ramps and stabilized at 4°C below the hot side at steady-state conditions during the high-temperature dwell.

The RDA data corresponding to the tool (hot) and window (cold) sides of the sample is shown in Figure 7b. The viscosity remained low during the temperature ramp, but rose abruptly after the gel point (indicated by square markers). At this point, the mismatch in viscosity between the hot and cold sides became significant. Due to a 13 minute lag in the onset of gelation on the cold side, the maximum viscosity difference was almost five orders of magnitude. This indicates that the sample did not cure uniformly, but rather experienced a “gelation boundary”, which began on the hot side of the part and moved through the thickness toward the colder side.

Figure 7c shows the mold cavity pressure (black), the pressure in the injector air supply line (green), and the “critical pressure” above which volatile release is suppressed (dashed line). The moments at which vacuum and positive pressure (300 kPa) were applied to the cavity and injector, respectively, are visible at 45-50 minutes. They correspond to the injection phase. Once injection



was complete, the supply pressure was increased to 450 kPa during the temperature ramp and dwell at 185°C. The cavity pressure after injection was initially below the supply level due to frictional losses within the injector, but slowly increased during the temperature ramp due to thermal expansion of the resin [25]. Once the final high-temperature dwell was reached, the cavity pressure began to decrease, and rapidly dropped below the critical pressure, as indicated by the dotted vertical line.

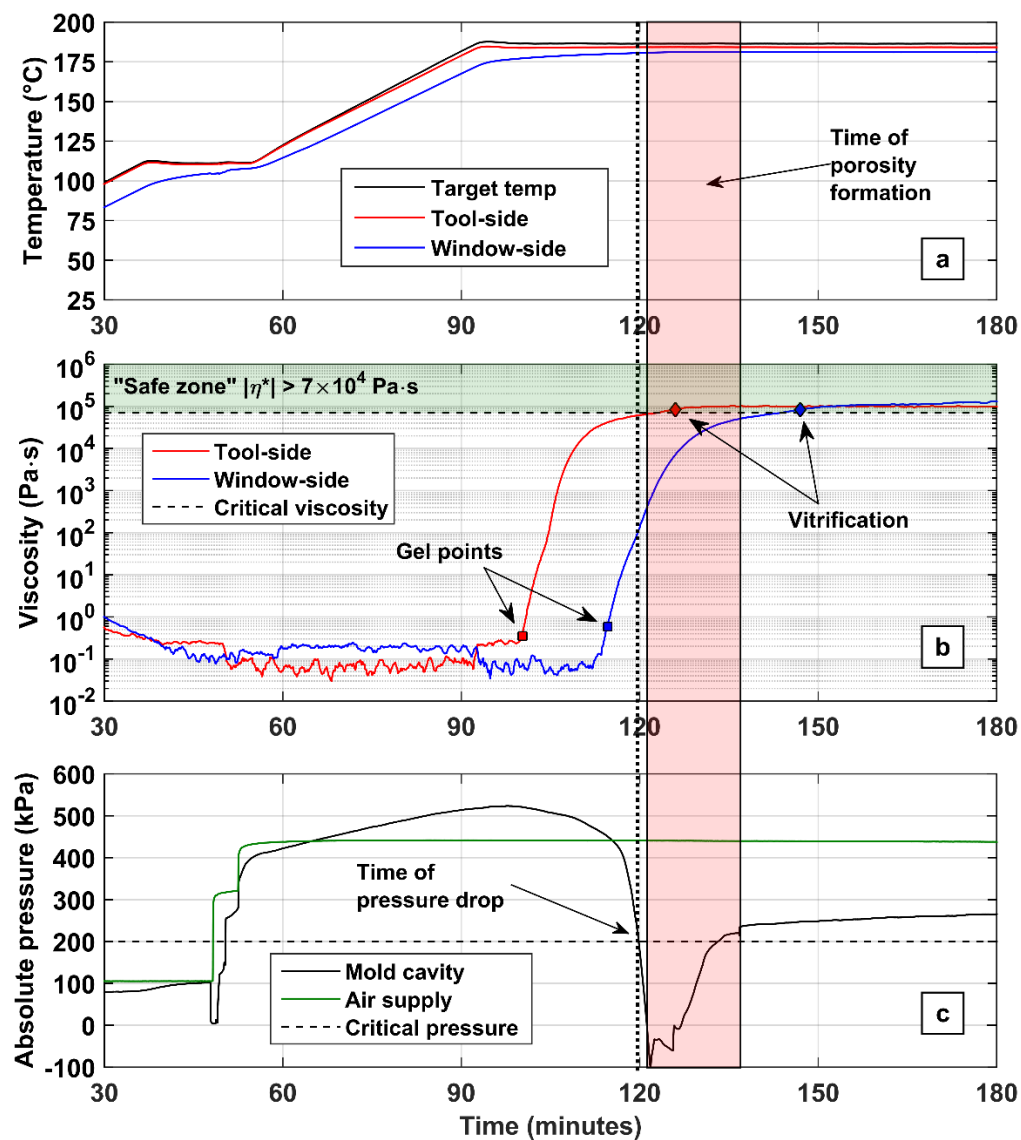


Figure 7: Temperature, viscosity, and pressure for formulation F1, Cycle A.



This pressure drop is caused by cure shrinkage – a decrease in specific volume due to polymer cross-linking – and is an unavoidable consequence of curing resin in a rigid, fixed-volume molding tool [25]. Because pressure is proportional to volumetric changes (by the bulk modulus), even a small amount of cure shrinkage can reverse the stress state within the curing resin from a state of hydrostatic compression to tension (assuming sufficient adhesion between the resin and mold surfaces). Initially after injection, cavity pressure is provided hydrostatically through the inlet. Once the resin near the inlet gels, the pressure in the rest of the mold cavity becomes isolated from the externally applied pressure, and instead becomes entirely governed by volumetric changes. The cumulative cure shrinkage of the resin, once the inlet has gelled, determines the timing of the pressure drop.

In the case of Figure 7, surface porosity occurred because of the relative timing of the pressure drop and the increasing viscosity at the coldest location of the mold cavity. The pressure drop occurred when the cold-side viscosity was in the vicinity of $100 \text{ Pa}\cdot\text{s}$, which is past the gel point, but far below the critical value of $7 \times 10^4 \text{ Pa}\cdot\text{s}$ that has been shown to suppress volatile release. The hot-side, meanwhile, had already reached a high viscosity level, and therefore did not off-gas.

Once the mold cavity pressure decreased below the critical value, voids began to form at the cold surface. The period of void formation was clearly observable through the window in the mold, and is indicated on Figure 7. Figure 8 shows a series of images recorded *in situ* for the same sample, beginning with an initially defect-free surface just before the pressure drop. Almost immediately after the pressure fell below the critical value, voids began to form and continued to grow for 15 minutes. All void growth finally ceased as the cold-side viscosity reached the “safe zone”, where the resin was nearly vitrified. In cases of extreme porosity such as in Figure 8, much of the surface separates from the tool face, clearly manifest through the window because of the change in refractive



index (compare Figure 8c and d), and accompanied by a concurrent spike/drop in measured cavity pressure (see Figure 7 at 136 minutes). The volatile gasses are less dense than the liquid resin, so their release at the cold surface relieves the tensile stresses generated by cure shrinkage. This phenomenon can be seen in Figure 7 by the gradual recovery in pressure during the time of porosity formation. Note that, since the pressure drop occurred when most of the resin was already approaching high viscosities (and due to the presence of the fibrous preform), the total volume of volatiles released was much lower than for the ambient-pressure neat resin samples (which began to grow bubbles earlier, during the ramp to the high-temperature dwell).



Figure 8: Surface porosity formation recorded in-situ for the composite sample with formulation F1, Cycle A. The thermocouple used to measure the window-side temperature history is visible in the center of the frame.



In summary, the tendency of this resin to exhibit surface porosity in RTM processing stems from a combination of two factors: significant potential for volatile release during cure, and rapid, highly temperature-dependent gelation, which increases the material sensitivity to in-mold temperature gradients. Additionally, the distribution of the porosity – concentrated on the cold surface – is determined by the direction of the temperature gradient.

3.3.2. Effect of Formulation and Cure Cycle

The following results illustrate the influence of cure kinetics on surface porosity, and reveal a strategy that can be used to minimize this type of defect. Figure 9 shows a comparison of the viscosity envelopes for the three samples cured using Cycle A, with the times corresponding to the pressure drops indicated by vertical dotted lines. Figure 10 shows the same type of data for samples with Cycle B.

The viscosity data shown for F1 in Figure 9 (Cycle A) is the same as from Figure 7. During the intermediate dwell of Cycle B at 130°C (Figure 10), formulation F1 remained inert and the viscosity did not increase. When the temperature was increased to 185°C, the F1 gelation profile was nearly identical to that of Cycle A, indicating that no significant cure progress occurred during the intermediate dwell. The cold-side viscosity at the time of the pressure drop was low in both cases, and accordingly, the porosity was most severe for these samples.

The viscosity envelopes for formulations F2 and F3 shown in Figure 9 display an onset of gelation at lower temperatures than for F1. Viscosity increased earlier with increasing catalyst concentration, but more importantly, the widths of the envelopes were reduced. Consequently, at the moment of the pressure drop, the cold-side viscosities were greater than for the sample with minimal catalyst (F1). As a result, the Cycle A-F2 and -F3 samples displayed almost an order of magnitude reduction in surface porosity compared to the baseline F1 formulation.

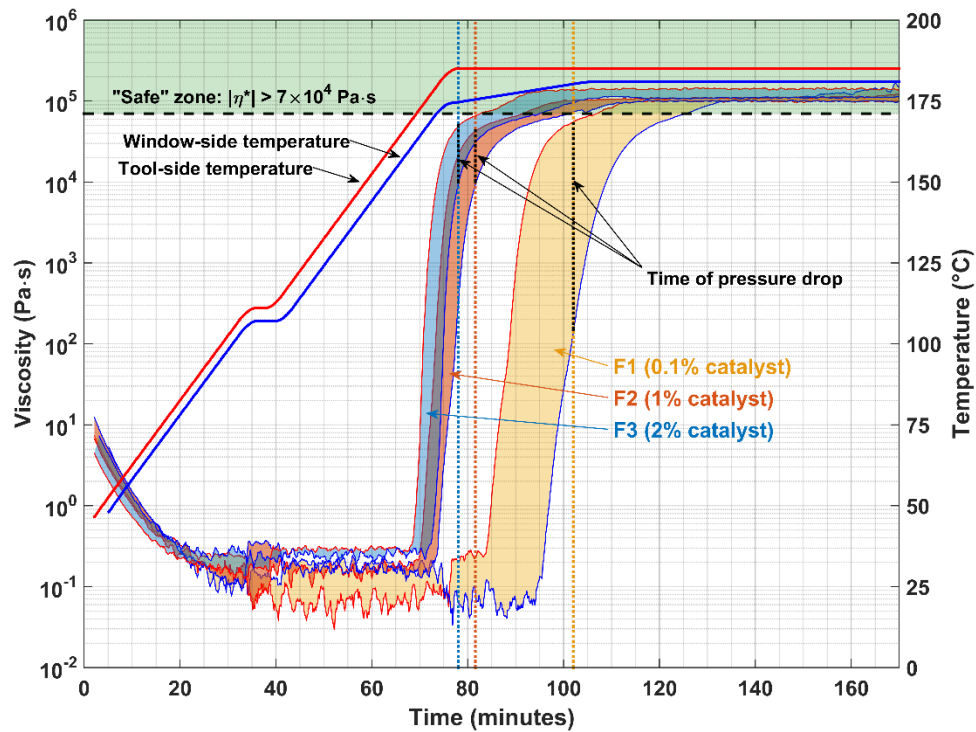


Figure 9: Viscosity envelopes for laminates cured with Cycle A.

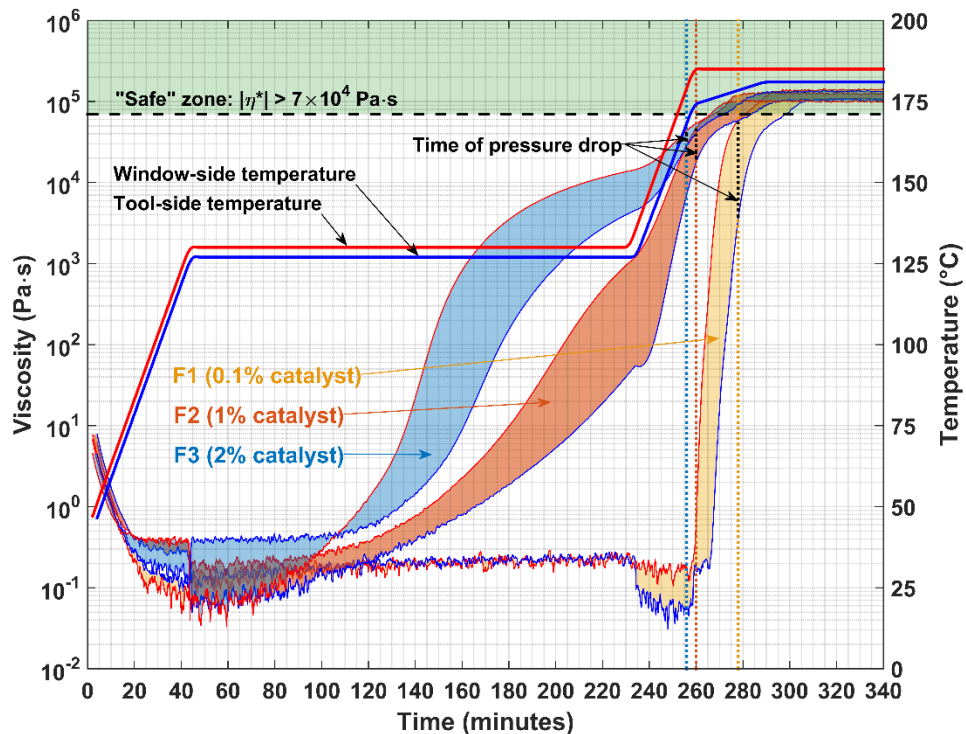


Figure 10: Viscosity envelopes for laminates cured with Cycle B.



The influence of the catalyst was even more pronounced for Cycle B (Figure 10), in which the F2 and F3 viscosities exhibited a progressive but limited increase during the intermediate temperature dwell. This prevented the through-thickness viscosity gradient from becoming as large as for Cycle A (or as for F1 under both cure cycles), once the temperature was increased towards 185°C. As expected, the cold-side viscosities during the pressure drops for F2 and F3 were greater in Cycle B than in Cycle A. Accordingly, these samples exhibited the lowest levels of surface porosity.

While the cold-side viscosity directly affects the release of resin volatiles at that surface, this parameter alone is not sufficient to fully explain the resulting surface porosity. For example, formulation F1 had a greater cold-side viscosity for Cycle B than for Cycle A at the time of the pressure drop, but the total defective surface area was greater for Cycle B. The explanation for this apparent discrepancy lies in the magnitude of the viscosity *gradient* between the hot and cold sides. After injection, uncured resin in the mold is initially under hydrostatic pressure. As the curing reaction progresses, cure shrinkage (generally assumed to progress linearly with degree-of-cure [24]) causes a decrease in specific volume and, in extremis, reverses the stress state from compressive to tensile. If a temperature gradient exists, then the shrinkage contribution of the hotter side to the total shrinkage is greater than that of the colder side, which has not progressed as far. If the imbalance in the progression of cure is sufficiently large, then the critical amount of total shrinkage to cause a pressure drop occurs when the cold-side viscosity remains low enough to allow volatile release. The greater the difference in viscosity between the hot and cold sides, the earlier the pressure drop occurs relative to the evolution of the cold-side viscosity, allowing more time for volatile release to occur before the critical viscosity is attained.



The relationship between the magnitude of the viscosity gradient at the moment of the pressure drop and the resulting surface porosity roughly follows an exponential trend, as shown in Figure 11. Formulation F1 exhibited the largest viscosity gradient and extensive surface porosity for both cure cycles. In comparison, F2 and F3 showed a significant reduction in defective surface area with Cycle A, and an even greater reduction with Cycle B.

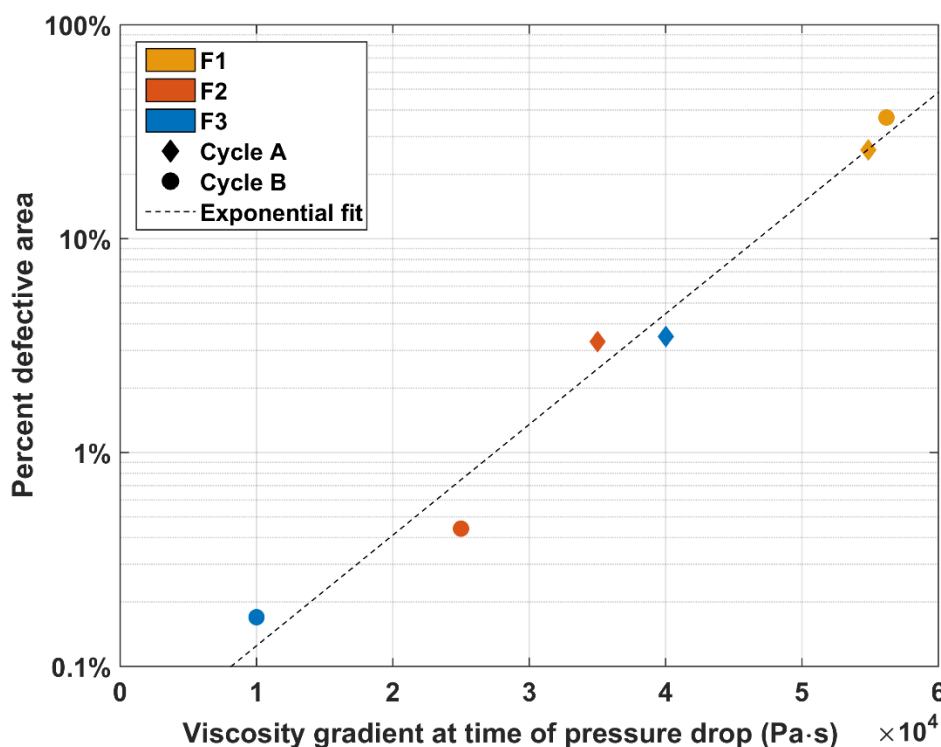


Figure 11: Comparison of the cold-side surface porosity of molded samples with the viscosity gradient at the time of the pressure drop.

The combination of increased catalyst loading and an intermediate temperature dwell in the cure cycle effectively prevents surface porosity, by allowing the resin to reach higher viscosities before the inevitable pressure drop. Cure shrinkage progresses only enough to cause pressure drops near the end of conversion, and the extent of conversion possible at 130°C is limited (exemplified by the decreasing slope of the viscosity envelope for F3 in Figure 10). The mold can therefore be held at



130°C with little risk of pressure loss, reducing the amount by which the cold-side viscosity lags when the RTM tool is ramped to the final dwell temperature.

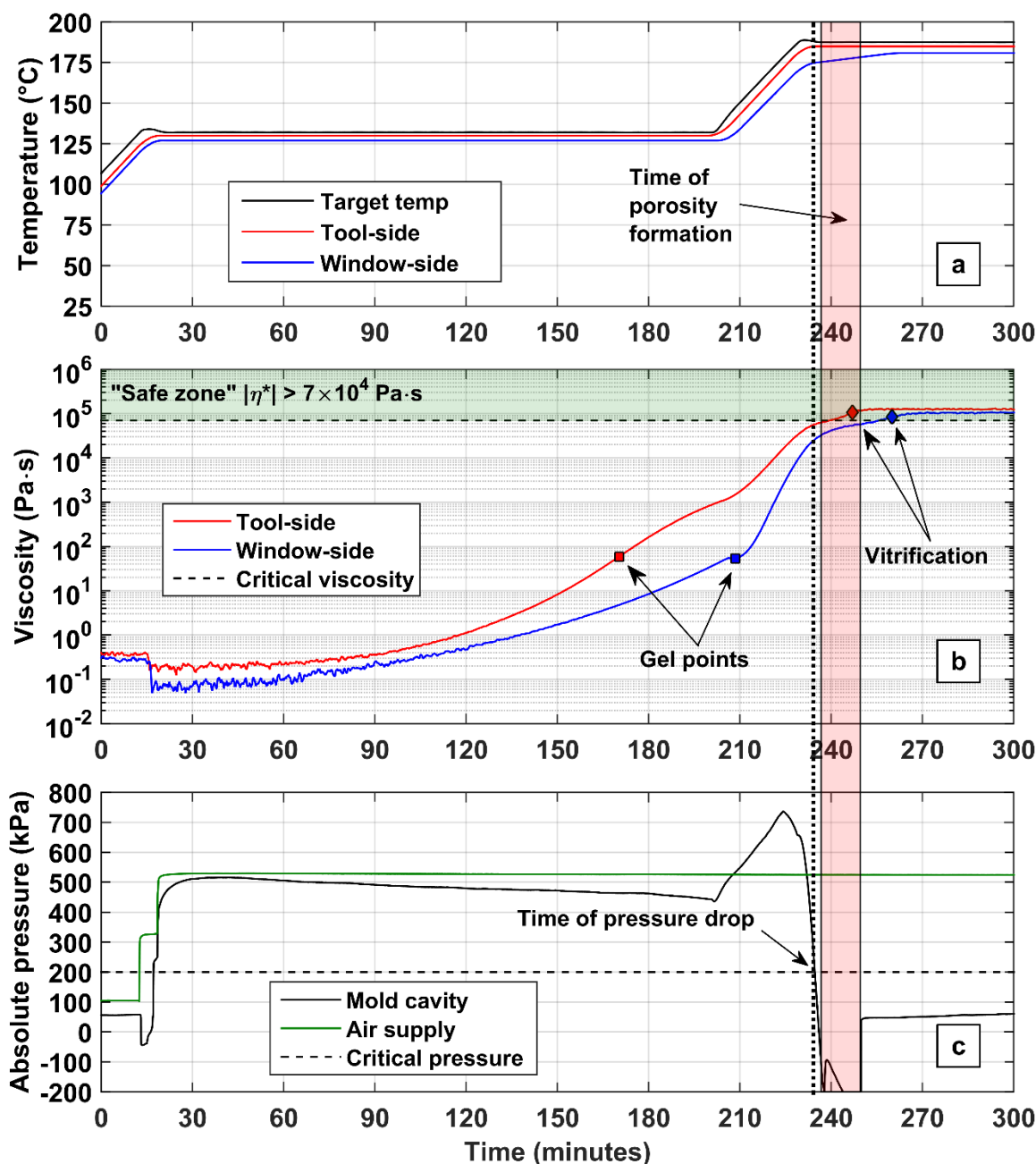


Figure 12: Temperature, viscosity, and pressure for formulation F2, Cycle B.

An additional effect of inducing gelation at a lower temperature is revealed by comparing the pressure histories of Figure 7 and Figure 12. In the former case, when the temperature is ramped to



185°C, the pressure increases only slightly (about 3 kPa/min). As the resin in the cavity undergoes thermal expansion, it can flow out through the constant-pressure inlet port to maintain equilibrium with the supply pressure. However, in Figure 12, during the final temperature ramp, the resin has already gelled and thus cannot flow. Consequently, thermal expansion causes a sharper pressure increase (about 16 kPa/min), an effect that can have multiple consequences. Firstly, the magnitude of the pressure spike is not easily predicted. This can cause dangerous stress levels in the molding tool, so care must be exercised not to exceed the maximum pressure allowed by the design of the tool. This is especially important when using brittle tool plates (i.e. glass), which can fracture catastrophically rather than simply yielding. Despite these concerns, thermal expansion is beneficial in that it counteracts the volumetric shrinkage induced by cure, making it possible to maintain cavity pressure after gelation (when externally applied pressure becomes ineffective). The thermally-induced pressure increase delays the cure-shrinkage-induced pressure drop, affording additional time for the resin to progress through the rubbery phase and near vitrification, where the potential for volatile release diminishes.

4. CONCLUSIONS

This work is part of a comprehensive effort to understand the relationships between resin properties, in-mold phenomena, and part quality for a next-generation blended resin system currently under development. In this study, we've sought to use a practical, experimental approach to reducing defect formation in this complex resin. A versatile tool was developed, allowing *in situ* process diagnostics to provide insights into what is generally a "black-box" process. By combining *in situ* data with volatile release criteria developed through thermal analysis, we describe the causes and mechanisms underlying volatile-induced surface porosity. In short, volatile-induced surface porosity can occur when curing resins with high volatility in a rigid mold cavity in which thermal gradients



exist, even if the temperature differences are relatively small. After the inlet gels, external hydrostatic pressure cannot be used to maintain cavity pressure, and cure shrinkage inevitably causes a pressure drop. Volatile release can then occur in colder zones within the cavity, where the resin has not yet vitrified.

The results demonstrate how several parameters strongly influence surface porosity, although there is room for further process refinement. The modified cure cycle B improves on the baseline case of ramping directly to the final high-temperature dwell, but the cycle is by no means optimized. A process that minimizes both surface porosity and total cycle time would be desirable from a manufacturing perspective. The ultimate goal is to find a robust solution, one that is insensitive to small deviations from the prescribed processing parameters, so that even in a larger RTM tool, which may have larger thermal gradients, surface porosity can still be prevented.

Note that in the molding tool used for this study, the thermal gradients were primarily through-thickness, acting as a simple 1-D “model case” for the phenomenon of surface porosity. In general, thermal gradients potentially include in-plane as well as through-thickness components. Although not described in detail here, preliminary tests using the same resins in a second, larger RTM (which contains substantial in-plane temperature gradients) have shown that the distribution of surface porosity is consistently correlated with the coldest zones in the mold cavity.

The effect of in-plane temperature gradients on pressure loss behavior, however, requires a more sophisticated description. For the one-dimensional case considered in the present study, we assume that the pressure detected by the sensor is transmitted through the thickness, i.e., that the pressure measured on the hot side is equal to that on the cooler side. For large RTM parts with in-plane temperature gradients, in-plane stresses can vary with location, so the “critical pressure” criterion for void formation would be useful only if applied locally. As a further complication, while the



specific volume of the resin is an intrinsic property, the total amount of shrinkage resulting in a pressure drop will vary between tools (depending part thickness, mold rigidity, etc.), potentially making the timing difficult to predict.

Despite the simplifications used in this study, lessons can be learned from the data to guide the processing for other resins and more complex geometries. First, the lag in the viscosity increase of the coldest region is directly related to porosity formation, so care should be exercised to minimize or avoid cold zones in all cases. Secondly, a two-dwell cure cycle has been shown to be effective at separating the cure reaction into multiple stages - first gelling the part while providing pressure externally, then maintaining pressure while in the rubbery phase (between the gel point and vitrification) by increasing the temperature, and lastly, reaching the final degree of cure after the pressure has dropped but volatile release is no longer possible. Because the improvement in surface quality comes at the expense of additional cycle time, increased catalyst concentrations can be employed to accelerate the first stage of cure. The limiting factor to this approach is the reduction in pot life, which may become dangerously short if the resin is highly catalyzed.

A generalized model to predict volatile-induced surface porosity for arbitrarily shaped parts would allow defect prediction and cure cycle optimization for parts manufactured under spatially-varying pressure and temperature fields. Such a model would require a description of heat transfer, thermochemical phenomena (degree of cure, viscosity), volumetric changes (thermal and chemical), and mechanical properties (at least bulk modulus, to predict pressure behavior based on volumetric changes). In this work, we experimentally determined and demonstrated the “critical pressure” and “critical viscosity” criteria, which could be applied to such a model to predict the timing, location, and severity of volatile-induced surface porosity.



Acknowledgements: The authors acknowledge financial and material support from the M.C. Gill Composites Center. Undergraduate research assistant Matthew Thomas contributed to the experimental characterization of the resin.

References:

- [1] Potter KD. The early history of the resin transfer moulding process for aerospace applications. *Compos Part A Appl Sci Manuf* 1999;30:619–21. doi:10.1016/S1359-835X(98)00179-1.
- [2] Kruckenberg T, Paton R. *Resin Transfer Moulding for Aerospace Structures*. Springer Netherlands; 1998. doi:10.1007/978-94-011-4437-7.
- [3] Pearce N, Guild F, Summerscales J. A study of the effects of convergent flow fronts on the properties of fibre reinforced composites produced by RTM. *Compos Part A Appl Sci Manuf* 1998;29:141–52. doi:10.1016/S1359-835X(97)00041-9.
- [4] Ruiz E, Achim V, Soukane S, Trochu F, Bréard J. Optimization of injection flow rate to minimize micro/macro-voids formation in resin transfer molded composites. *Compos Sci Technol* 2006;66:475–86. doi:10.1016/j.compscitech.2005.06.013.
- [5] Leclerc JS, Ruiz E. Porosity reduction using optimized flow velocity in Resin Transfer Molding. *Compos Part A Appl Sci Manuf* 2008;39:1859–68. doi:10.1016/j.compositesa.2008.09.008.
- [6] Liu B, Bickerton S, Advani SG. Modelling and simulation of resin transfer moulding (RTM) - Gate control, venting and dry spot prediction. *Compos Part A Appl Sci Manuf* 1996;27:135–41. doi:10.1016/1359-835X(95)00012-Q.
- [7] Lundström T, Gebart B. Influence from process parameters on void formation in resin transfer molding. *Polym Compos* 1994;15:25–33. doi:10.1002/pc.750150105.
- [8] Pollard HJ, Rees J. Improvements in or relating to the moulding of articles from thermosetting resins and fibrous material. British Patent Specification 778,683, 1956.
- [9] Varna J, Joffe R, Berglund LA, Lundström TS. Effect of voids on failure mechanisms in RTM laminates. *Compos Sci Technol* 1995;53:241–9. doi:10.1016/0266-3538(95)00024-0.
- [10] Haider M, Hubert P, Lessard L. An experimental investigation of class A surface finish of composites made by the resin transfer molding process. *Compos Sci Technol* 2007;67:3176–86. doi:10.1016/j.compscitech.2007.04.010.
- [11] Kardos JL, Duduković MP, Dave R. Void growth and resin transport during processing of thermosetting — Matrix composites. *Adv. Polym. Sci.*, 1986, p. 101–23. doi:10.1007/3-540-16423-5_13.
- [12] Wood JR, Bader MG. Void control for polymer-matrix composites (1): Theoretical and experimental methods for determining the growth and collapse of gas bubbles. *Compos Manuf* 1994;5:139–47. doi:10.1016/0956-7143(94)90023-X.



- [13] Ledru Y, Piquet R, Schmidt F, Michel L, Bernhart G. Modeling of void growth mechanisms during the manufacturing of composite laminates. Proc. 9th Int. Conf. Flow Process. Compos. Mater., Montréal, Canada: 2008.
- [14] Ledru Y, Bernhart G, Piquet R, Schmidt F, Michel L. Coupled visco-mechanical and diffusion void growth modelling during composite curing. *Compos Sci Technol* 2010;70:2139–45. doi:10.1016/j.compscitech.2010.08.013.
- [15] Lundström TS. Measurement of void collapse during resin transfer moulding. *Compos Part A Appl Sci Manuf* 1997;28:201–14. doi:10.1016/S1359-835X(96)00109-1.
- [16] Afendi M, Banks WM, Kirkwood D. Bubble free resin for infusion process. *Compos Part A Appl Sci Manuf* 2005;36:739–46. doi:10.1016/j.compositesa.2004.10.030.
- [17] Eom Y, Boogh L, Michaud V, Sunderland P, Månson J-A. Stress-initiated void formation during cure of a three-dimensionally constrained thermoset resin. *Polym Eng Sci* 2001;41:492–503. doi:10.1002/pen.10746.
- [18] Eom Y, Boogh L, Michaud V, Månson J. A structure and property based process window for void free thermoset composites. *Polym Compos* 2001;22:22–31. doi:10.1002/pc.10512.
- [19] Wisnom MR, Gigliotti M, Ersoy N, Campbell M, Potter KD. Mechanisms generating residual stresses and distortion during manufacture of polymer-matrix composite structures. *Compos Part A Appl Sci Manuf* 2006;37:522–9. doi:10.1016/j.compositesa.2005.05.019.
- [20] Merzlyakov M, McKenna GB, Simon SL. Cure-induced and thermal stresses in a constrained epoxy resin. *Compos Part A Appl Sci Manuf* 2006;37:585–91. doi:10.1016/j.compositesa.2005.05.013.
- [21] Haider M, Hubert P, Lessard L. Cure shrinkage characterization and modeling of a polyester resin containing low profile additives. *Compos Part A Appl Sci Manuf* 2007;38:994–1009. doi:10.1016/j.compositesa.2006.06.020.
- [22] Ramos J a., Pagani N, Riccardi CC, Borrajo J, Goyanes SN, Mondragon I. Cure kinetics and shrinkage model for epoxy-amine systems. *Polymer (Guildf)* 2005;46:3323–8. doi:10.1016/j.polymer.2005.02.069.
- [23] Li C, Potter K, Wisnom MR, Stringer G. In-situ measurement of chemical shrinkage of MY750 epoxy resin by a novel gravimetric method. *Compos Sci Technol* 2004;64:55–64. doi:10.1016/S0266-3538(03)00199-4.
- [24] Nawab Y, Shahid S, Boyard N, Jacquemin F. Chemical shrinkage characterization techniques for thermoset resins and associated composites. *J Mater Sci* 2013;48:5387–409. doi:10.1007/s10853-013-7333-6.
- [25] Kendall KN, Rudd CD, Owen MJ, Middleton V. Characterization of the resin transfer moulding process. *Compos Manuf* 1992;3:235–49. doi:10.1016/0956-7143(92)90111-7.
- [26] Boyard N, Millischer a., Sobotka V, Bailleul JL, Delaunay D. Behaviour of a moulded composite part: Modelling of dilatometric curve (constant pressure) or pressure (constant volume) with temperature and conversion degree gradients. *Compos Sci Technol* 2007;67:943–54. doi:10.1016/j.compscitech.2006.07.004.



- [27] Landry B, Hubert P. Experimental study of defect formation during processing of randomly-oriented strand carbon/PEEK composites. *Compos Part A Appl Sci Manuf* 2015;77:301–9. doi:10.1016/j.compositesa.2015.05.020.
- [28] Landry B, Hubert P. Modelling Pressure Distribution During Cooling of Randomly-Oriented Strand Carbon/PEEK Composites. *Proc. 20th Int. Conf. Compos. Mater.*, Copenhagen, Denmark: 2015.
- [29] Pupin C, Ross A, Ruiz E, Billotte C, Rietsch J-C, Bricourt P, et al. Porosity Control by Process Parameters. *Proc. 20th Int. Conf. Compos. Mater.*, Copenhagen, Denmark: 2015.
- [30] Ishida H, Allen DJ. Mechanical characterization of copolymers based on benzoxazine and epoxy. *Polymer (Guildf)* 1996;37:4487–95. doi:10.1016/0032-3861(96)00303-5.
- [31] Rimdusit S, Tiptipakorn S, Jubsilp C, Takeichi T. Polybenzoxazine alloys and blends: Some unique properties and applications. *React Funct Polym* 2013;73:369–80. doi:10.1016/j.reactfunctpolym.2012.04.022.
- [32] Anders M, Lo J, Centea T, Nutt SR. Minimizing Volatile-Induced Surface Porosity in RTM via Material and Process Optimization. *Proc. 20th Int. Conf. Compos. Mater.*, Copenhagen, Denmark: 2015.
- [33] Lo J, Anders M, Centea T, Nutt S. Multi-Scale Material and Process Characterization for Resin Transfer Molding: Case Study for a Blended Epoxy/Polybenzoxazine Resin. *Proc. 20th Int. Conf. Compos. Mater.*, Copenhagen, Denmark: 2015.
- [34] Lo J, Anders M, Centea T, Nutt SR. The Effect of Process Parameters on Volatile Release for a Benzoxazine-Epoxy RTM Resin *unpublished manuscript JCOMA-15-1197 (currently under review). *Compos Part A Appl Sci Manuf* 2015.
- [35] Winter HH, Mours M. Rheology of Polymers Near Liquid-Solid Transitions. *Neutron Spin Echo Spectrosc. Viscoelasticity Rheol.*, vol. 134, Berlin, Heidelberg: Springer Berlin Heidelberg; 1997, p. 165–234. doi:10.1007/3-540-68449-2_3.
- [36] Bilyeu B, Brostow W, Menard KP. Separation of gelation from vitrification in curing of a fiber-reinforced epoxy composite. *Polym Compos* 2002;23:1111–9. doi:10.1002/pc.10505.